Alignment of Light and Mass in Lensing Galaxies

Claudio Bruderer[1]⋆, J. I. Read[1,2], P. Saha[3], J. Coles[4]

[1] *Institute for Astronomy, Department of Physics, ETH Zürich, Wolfgang-Pauli-Strasse 27, CH-8093 Zürich, Switzerland*
[2] *Department of Physics, University of Surrey, Guildford, GU2 7XH, UK*
[3] *Institute for Theoretical Physics, University of Zürich, Winterthurerstrasse 190, 8057 Zürich, Switzerland*
[4] *Department of Biology and Health, Versailles Saint-Quentin-en-Yvelines University, France*

21 July 2014

ABSTRACT
Understanding the structure and properties of galaxies today is essential to understand how galaxies formed. This poses a larger problem to us than one might imagine. Especially constraining the dark matter distribution in galaxy halos is not trivial. There are only a few methods to directly estimate this distribution. One of them is strong gravitational lensing, an effect caused by all of mass. This phenomenon allows constraining the gravitational potential of lens galaxies and thus the mass distribution. With knowledge of the light distribution it is possible to disentangle the dark matter and baryonic mass components and study their properties. We use the newly-developped nonparametric framework *GLASS* to model the mass distribution of a total of 15 strong gravitational lensing galaxies, most of which are early-type galaxies, for which we have information on the baryonic mass distribution. We are thus able to separate the mass components. By using a simple shape measure, namely the inverse of the moment of inertia tensor, we can analyze the shapes of the distributions. Analyzing the alignments between the semi-major axes of the distributions, we find that there can be significant misalignments and also cases of alignment between the semi-minor and semi-major axes. Mass thus need not follow light. Furthermore, the ellipticities of the dark matter distributions are always smaller than the baryonic mass distributions. Dark matter halos tend to be more spherical than the light distribution of the galaxy. We also consider the environment of the lenses. We find that lenses in denser environments tend to be more misaligned with either the semi-major or semi-minor axis. Additionally, the semi-major axis of lenses lying in groups or clusters of the dark matter halo might be oriented in direction of the centroid.

Key words: asdf....

1 INTRODUCTION

Content:

• Understand galaxy structure (→ Links to galaxy evolution?)
• Relevant for weak lensing (Intrinsic alignments)
• Strong lensing reacts purely due to total mass distribution → Can disentangle light and mass
• Free-form modelling (or #constraints ≪ #dof)

To Do:

• Rewrite introduction and change pitch to: Understand mass and light alignment, understand effect on IA

Gravitational lensing is one of the few phenomena that allow probing the matter distribution directly. It makes no distinction between baryonic and dark matter, both components act on light rays in the same way. Gravitational lensing is therefore somewhat special as it allows to *see* dark matter, if we are able to separate the two components. Therefore studying these effects allows us to probe dark matter and its properties. We are typically interested in measuring its distribution, how it clusters, its connection to structure formation, and of course its nature. With strong gravitational lensing galaxies we are effectively probing the matter distribution on relatively small scales. Thus, much insight could be gained in how galaxies form and how they are structured.

The main challenges are however first, estimating the baryonic mass distribution such that the two components can be disentangled (see e.g. Leier (2011)), and second, modelling the lens, i.e. the mass distribution. This work focuses purely on the second aspect. There are in general two classes of methods to reconstruct gravitational lenses, parametric and nonparametric methods. A comparison of these two

⋆ E-mail: claudio.bruderer@phys.ethz.ch

classes of methods can be found in Coe et al. (2008). Parametric methods assume a distribution, which depends only on few parameters, such that the problem is well constrained and a best-fitting model can be found. They are computationally cheap, but on the other hand the assumption of a distribution might bias the result (CITATION NEEDED!). Nonparamatric (or free-form) methods assume a set of basis functions and find valid solutions in terms of linear superpositions of these functions. The problem is largely underconstrained. Due to the fact that there is no a priori reason to prefer specific mass models, given that they all satisfy certain prior conditions and reproduce the same gravitational lensing effects, over others, the best-fitting model is of little interest. Much more important is to explore many models and look at the properties of all the models in the ensemble. Typically high-dimensional parameter spaces, which describe all allowed models, need to be sampled in a uniform and uncorrelated way to generate a representative ensemble of solutions. The computational cost of these methods is usually much higher (Coles 2008; Lubini & Coles 2012).

With these tools, we can start answering the long-standing question whether mass follows light. It is a well-known fact that for observations to match for example rotation curves of galaxies, the radial density profiles of baryonic mass and dark matter differ. The question is however whether baryonic mass and dark matter need to be aligned and the ellipticities need to agree. If this is not the case, then this needs to be explained by mechanism and effects that produce and sustain these different properties. Especially the environment of lenses might play a significant role (CITATION NEEDED!). It is furthermore unclear whether modified gravity theories could explain possible misalignments between mass and light.

There were already attempts to analyze the alignment of light and mass. Keeton et al. (1997) use Singular Isothermal Spheres (SIS) with an external shear term and Singular Isothermal Ellipsoids (SIE) (e.g. Kormann et al. (1994)) without external shear to model the mass distribution. Applying this to a sample of 17 lenses, they find a strong correlation between light and dark matter distributions, if there is no strong external perturbation, with only a small scatter of less than $10°$. They find however no correlation between the axis ratios of the distributions.

Later on, Koopmans et al. (2006) and Gavazzi et al. (2012) analyzing lens samples of similar sizes and Treu et al. (2009) analyzing a lens sample containing even 70 galaxies also looked for misalignments. They all use SIEs to model the mass distributions. Only Gavazzi et al. (2012) however include an external shear contribution in case more information is available. They neglect the external shear although Keeton et al. (1998) find that SIEs with an independent external shear term fit the data better. They find reasonable alignments, the scatter is however larger than the one found in Keeton et al. (1997). Gavazzi et al. (2012) find a rms scatter of $25°$ for the whole sample. Even after dropping the almost spherical lenses, the rms scatter is still $18°$. They attribute this to a significant external shear contribution. Treu et al. (2009) even find a significant correlation between the misalignment and the local and global environment. In general, lenses in overdense environments seem to be more likely to be misaligned. Treu et al. (2009) and Gavazzi et al.

(2012) also find a correlation with a large scatter between the ellipticities of the light and dark matter distributions.

Contrary to earlier approaches, we choose to use a nonparametric modelling technique. We use a pixel-based (see e.g. Saha & Williams (1997)) lens reconstruction framework called *GLASS* (Lubini & Coles 2012). We apply this successfully on a sample of 15 strong gravitational lensing galaxies using stellar mass data of Leier (2011). Thus, we can disentangle dark and luminous matter and look at the shapes and alignments of these distributions. We can also look at the ellipticities of the reconstructed lenses and compare them to the ones of the stellar distribution. Furthermore, we discuss the environments of these lenses, as they might affect some properties of gravitational lenses in a significant way (Momcheva et al. 2006; Wong et al. 2011). We think that we have enough statistics to make claims about misalignments between the dark matter halo and the stellar mass distribution, and how the halo is oriented compared to the environment.

In Section 2 we present the lens sample and important properties of each lens. In Section 3 we present the reconstruction method we use and our shape measure. Section 4 consists of the results of this analysis. We show the relations we find between misalignment, ellipticities, and the environment.

2   DATA

Content:

- Describe data set (why this data set, special features of galaxies (environment: y/n/unknonwn, elliptical/disk))
- Maybe lose a couple of words on SPS?

  To Do:

- Rephrase
- Add maybe something on SPS

The pixelated stellar mass maps we use, were reconstructed by Leier (2011). For each pixel the surface brightness was compared with stellar mass-to-light ratios, which were determined by stellar population synthesis models. This technique allows estimating the stellar mass in these pixels. Further details on this method can be found in Leier (2011), Ferreras et al. (2005), Ferreras et al. (2008).

Our sample originally consisted of 21 galaxies, identical to the one in Leier (2011) and Leier et al. (2011). As the lenses *HS0818+1227*, *SBS1520+530*, *B1600+434*, *B1608+656* proved too difficult to reconstruct, we dropped them from this analysis. The final sample consists thus of 17 galaxies. Most of these lenses are early-type galaxies except *B1030+074*, *B1152+200*, and *Q2237+030*. All lenses can also be found in the gravitational lens database *CASTLES*. Characteristics and references of each lens in the sample are listed below. Table 1 contains all the redshifts and the type of the lenses, Table 2 lenses with environment information, and Table 3 lenses with measured time delays.

Q0047-2808 (hereafter *Q0047*) is a luminous early-type galaxy (Warren et al. 1996). Wong et al. (2011) find a group of 9 members all of which they spectroscopically confirm.

Lens	z_L	z_S	Type	Lens	z_L	z_S	Type
Q0047	0.48	3.60	Quad	HE1104	0.73	2.32	Double
Q0142	0.49	2.72	Double	PG1115	0.31	1.72	Quad
MG0414	0.96	2.64	Quad	B1152	0.44	1.02	Double
B0712	0.41	1.34	Quad	B1422	0.34	3.62	Quad
RXJ0911	0.77	2.80	Quad	MG2016	1.01	3.27	Quad[1]
BRI0952	0.63	4.50	Double	B2045	0.87	1.28	Quad
Q0957	0.36	1.41	Double	HE2149	0.60	2.03	Double
LBQS1009	0.87	2.74	Double	Q2237	0.04	1.69	Quad
B1030	0.60	1.54	Double				

Table 1. List of all the lenses in the sample and their properties. Data is taken from *CASTLES* and Leier (2011). The angles are measured north-through-east.

[1] Two images merge, thus only three images can be resolved.

Lens	Environment[a]	Group/Cluster centroid[b] $\Delta\alpha$ ["]	Group/Cluster centroid[b] $\Delta\delta$ ["]	Other galaxy $\Delta\alpha$ ["]	Other galaxy $\Delta\delta$ ["]	References[c]
Q0047	G(9)	3.6 ± 15.6	43.2 ± 28.8	...	...	1
MG0414	2	...	...	-0.4	1.5	2
B0712	2	...	...	47	-91	3
RXJ0911	C	-12.0	-39.8	...	...	4
Q0957	C	...	...	...	...	5
B1030	2	...	...	-9.8	8.5	6
PG1115	G(13)	-10.8 ± 21.0	-3.6 ± 15.6	...	...	1
B1422	G(17)	61.2 ± 25.2	-10.8 ± 23.4	...	...	1
B1608	G(8)	-0.7	8.0	...	...	9
MG2016	C(69)	...	...	...	...	10
HE2149	G	-36.6	14.2	...	...	11

Table 2. List of lenses lying in a group or cluster environment, or that have a companion.

[a] G stands for group, C for cluster, and 2 means that the lens has a companion galaxy. If known, the number of member galaxies including the lens is given.

[b] If not stated differently, the centroid positions are luminosity-weighted estimates.

[c] References for the centroid estimates we used.

1: Wong et al. (2011); 2: Schechter & Moore (1993); 3: Fassnacht & Lubin (2002); 4: Morgan et al. (2001); 5: Chartas et al. (1998); 6: Lehár et al. (2000); 7: Auger et al. (2008); 8: Auger et al. (2007); 9: Toft et al. (2003); 10: Williams et al. (2006); 11: Williams et al. (2006)

Q0142-100 (hereafter *Q0142*) is a passively evolving early-type galaxy according to (Lehár et al. 2000; Eigenbrod et al. 2007).

MG0414+0534 (hereafter *MG0414*) is a passively evolving early-type galaxy (Tonry & Kochanek 1999). Schechter & Moore (1993) find a very close luminous satellite galaxy north-west of the lens. Due to the proximity of this satellite, we include it as a point mass in our analysis.

B0712+472 (hereafter *B0712*) is an early-type galaxy (Fassnacht & Cohen 1998). Another galaxy, 102" to the south-east seems to be at a similar redshift (Fassnacht & Lubin 2002). There is also a group of 10 galaxies at a lower redshift.

RXJ0911+0551 (hereafter *RXJ0911*) is an almost circular early-type galaxy (Sluse et al. 2012). It has measured time delays (Hjorth et al. 2002) and lies on the outskirts of a cluster (Morgan et al. 2001). This cluster seems to be rather complex. Possibly it is not dynamically relaxed, although X-ray emission can be detected. Analysis of this emission yields a temperature of 2.3 keV. There is also a satellite galaxy to the north-west direction (Kneib et al. 2000).

BRI0952-0115 (hereafter *BRI0952*) is an early-type galaxy (Lehár et al. 2000; Eigenbrod et al. 2007). Momcheva et al. (2006) find that the lens lies in a poor group of 5 mem-

bers. However, a redshift of $z = 0.41$ was used. According to Eigenbrod et al. (2007), the redshift is more likely to be $z = 0.632$. They also find a system of 2 or 3 other galaxies at a slightly higher redshift of which the lens could be part of. The required external shear could be explained easily by a cosmic contribution (Lehár et al. 2000). Therefore, we treat this lens as an isolated object.

Q0957+561 (hereafter *Q0957*) is a cD galaxy lying close to the center of a cluster with a high sprial galaxy-fraction (e.g. Garrett et al. (1992); Angonin-Willaime et al. (1994); Chartas et al. (1998)). Due to the large image separation, large physical scales are probed. As listed in Table 3 of Keeton et al. (2000), the position angles to the center of the cluster of earlier lens reconstructions range between 51.8 deg and 67.8 deg measured north-through-east. These results are consistent with the center of the X-ray emission from the cluster (Chartas et al. 1998). The lens has a measured time delay (e.g. Shalyapin et al. (2012)). They however also find a three-day lag between the g- and r-bands, and the estimates do not agree at the 2σ-level. They argue that this effect can be accounted for by the presence of a substructure and chromatic dispersion. We find that the results do not change significantly for either estimate and choose therefore the g-band measurement.

Lens	Time delays [d]			References
RXJ0911	$\Delta t_{BA} = 146 \pm 4$	...	...	1
Q0957	$\Delta t_{BA} = 416.5 \pm 1.0^a$	$\Delta t_{BA} = 420.6 \pm 1.9^b$	...	2
HE1104	$\Delta t_{BA} = 162.2^{+6.3}_{-5.9}$	...	...	3
PG1115	$\Delta t_{BA} = 12.0^{+2.4}_{-2.0}$	$\Delta t_{DC} = 4.4^{+3.2}_{-2.4}$	...	4
B1608	$\Delta t_{BA} = 31.5^{+2}_{-1}$	$\Delta t_{CA} = 36.0 \pm 1.5$	$\Delta t_{DA} = 77.0^{+2}_{-1}$	7
HE2149	$\Delta t_{BA} = 103 \pm 12$	...	...	8

Table 3. Lenses with measured time delays. Δt_{BA} corresponds to the time delay between the images A and B with A leading.
[a] measured in the g-band
[b] measured in the r-band
1: Hjorth et al. (2002); 2: Shalyapin et al. (2012); 3: Morgan et al. (2008); 4: Tsvetkova et al. (2010); 5: Eulaers & Magain (2011); 6: Burud et al. (2000); 7: Fassnacht et al. (2002); 8: Burud et al. (2002)

LBQS1009-0252 (hereafter *LBQS1009*) is probably an early-type galaxy (Lehár et al. 2000). Faure et al. (2004) find no significant galaxy overdensity near the lens.

B1030+074 (hereafter *B1030*) appears to have some substructure (Xanthopoulos et al. 1998). Lehár et al. (2000) conclude that there are two distinct galaxies. The main one is a red, early-type galaxy. The other component seems to be fitted well by an exponential disk galaxy. They also conclude that no firm statements about the environment can be made. Although there is another galaxy nearby, it is too blue to be an early-type galaxy and thus they cannot estimate its shear contribution.

HE1104-1805 (hereafter *HE1104*) is probably an early-type galaxy (Lehár et al. 2000; Courbin et al. 2000) and has measured time delays (Morgan et al. 2008). Lehár et al. (2000) also seem to find a group environment. Faure et al. (2004) however conclude that the photometric redshift measurements of these galaxies indicate that they are at a higher redshift and rather associated with the source. Nonetheless, their lens models, parametric and free-form, all require strong external shear.

PG1115+080 (hereafter *PG1115*) is an early-type galaxy (Yoo et al. 2005). It has measured time delays. We use recent estimates of the time delays by Tsvetkova et al. (2010) which differ significantly from traditional values by e.g. Barkana (1997). Momcheva et al. (2006) and Wong et al. (2011) analyzed the environment of the lens thouroughly. It is part of a small group of 13 members. Grant et al. (2004) detect also X-ray emission from the corresponding group, which yields a temperature of 0.8 keV.

B1152+200 (hereafter *B1152*) seems to have a color consistent with a late-type or an irregular galaxy (Toft et al. 2000). Not much seems to be known about the environment of the lens.

B1422+231 (hereafter *B1422*) is an early-type galaxy (Impey et al. 1996). Although there are measured time delays by Patnaik & Narasimha (2001), they are probably not to be trusted too much as they deviate significantly from theoretical expectations in Raychaudhury et al. (2003). An accurate measurement of the time delays would require time delay measurements on the scale of hours. Momcheva et al. (2006) find a group environment with 16 spectroscopically confirmed member galaxies. Using newer data Wong et al. (2011) find an additional member. Grant et al. (2004) also detect X-ray emission from the corresponding group at a temperature of 1.0 keV.

MG2016+112 (hereafter *MG2016*) is a giant elliptical galaxy (Lawrence et al. 1984; Schneider et al. 1986). It is the farthest lens we consider in this sample. It lies in a cluster which consists of 69 probable member galaxies (Toft et al. 2003). The clusters shows a high density of galaxies close to the lens in a south-east direction.

B2045+265 (hereafter *B2045*) is probably an elliptical galaxy (McKean et al. 2007). Fassnacht et al. (1999) initially classified the galaxy as a late-type Sa galaxy, the velocity dispersion however seems too high. As the source redshift is rather low, a large lens mass is needed. McKean et al. (2007) therefore conclude that it is more likely an elliptical galaxy. To the west of the lens, Fassnacht et al. (1999) find that a group at a similar redshift as the lens. McKean et al. (2007) also find evidence for a dwarf satellite galaxy.

HE2149-2745 (hereafter *HE2149*) is an early-type galaxy (Eigenbrod et al. 2007) and has a measured time delay (Burud et al. 2002). There is some uncertainty in estimating the lens' redshift. Initial estimates by Wisotzki et al. (1996) and Kochanek et al. (2000) found a probable redshift range of $\sim 0.2 - 0.5$. By cross-correlating the lens spectrum with a template spectrum of an elliptical galaxy, Burud et al. (2002) find that the redshift probably lies in the range $0.49 \leqslant z \leqslant 0.60$, with the most likely redshift $z = 0.495 \pm 0.01$. Eigenbrod et al. (2007) however find that the redshift is more likely to be $z = 0.603 \pm 0.001$. This would probably make the lens part of a poor group found by Momcheva et al. (2006) and Williams et al. (2006). They also find two other groups at lower redshifts.

Q2237+030 (hereafter *Q2237* or *2237*) is a barred spiral (Yee 1988). With only a redshift of $z = 0.04$ it is the closest lens of the sample. Due to the low redshift, the probed physical scales are quite small. No further inquiries into the environment were made.

Further information about the sample can be found in Leier (2011), Leier et al. (2011), and Sluse et al. (2012).

3 METHOD

3.1 GLASS

Content:

- Describe code briefly
- Mention PixeLens and two other GLASS papers

To Do:

• Rephrase
• To avoid repetition, check what is really relevant for this paper, and for what we can just reference the other two GLASS papers
• Check that same parameter names are used as in the other papers

In this work we use the new free-form lens modelling framework *GLASS* (Lubini & Coles 2012). As its predecessor *PixeLens* (Saha & Williams 2004), it generates a pixelated mass map of a lens reproducing the image positions perfectly. Using pixels the arrival time surface for a source at position $\boldsymbol{\theta}_S$, taking the geometric and Shapiro contributions to the time delay into account, can be expressed in terms of the surface mass density rescaled by the critical density Σ_{crit} of the n-th pixel κ_n and the contribution to the gravitational potential of this pixel ψ_n (Saha & Williams 1997)

$$\tau(\boldsymbol{\theta}) = \frac{1}{2}|\boldsymbol{\theta}|^2 - \boldsymbol{\theta} \cdot \boldsymbol{\theta}_S - \sum_n \kappa_n \psi_n(\boldsymbol{\theta}). \qquad (1)$$

According to Fermat's principle, lensed images appear where the arrival time surface takes on extremal values $\nabla \tau(\boldsymbol{\theta}) = 0$. Thus, the image positions fulfil

$$\boldsymbol{\theta} - \boldsymbol{\theta}_S - \sum_n \kappa_n \alpha_n = 0, \qquad (2)$$

where α_n is the contribution to the bending angle of the n-th pixel. For pixels, α_n and ψ_n can be described by analytic formulae (Saha & Williams 1997). Reconstructing the lens, i.e. describing the surface mass density in every pixel, reduces thus to finding sets of coefficients $\{\kappa_n\}$ of these functions. As the number of pixels, which sets the resolution, is by far larger than the number of constraint equations in free-form modelling, this problem is highly underconstrained. The number of pixels is typically 100. We note that the equation is linear in κ_n. Also additional constraints on the lens such as individual time delays between images and their order and other priors we impose are linear. The volume of allowed solution is thus a high-dimensional polytope.

A fundamental difficulty in mass modelling is the non-uniqueness of solutions. They are not only not unique, every configuration which fulfils the equation is also equally probable. Therefore, this polytope needs to be sampled in a uniform way to analyze the full range of solutions. Due to the high dimensionality, sophisticated sampling methods of such volumes are required. *GLASS* and *PixeLens* differ in the method they use to sample such spaces. Coles (2008) and Lubini & Coles (2012) show that *PixeLens* does not produce uncorrelated random samples. They propose therefore a new sampling algorithm. They prove that generic high-dimensional polytopes indeed are sampled in a much more uniform way. Models in *GLASS* are generated using a MCMC-method with a Metropolis-Hastings algorithm. A new step x_{i+1} of the Markov chain is accepted with the probability

$$\alpha = \min\left(1, \frac{P(x_{i+1})Q(x_i, x_{i+1})}{P(x_i)Q(x_{i+1}, x_i)}\right), \qquad (3)$$

where $P(x)$ is the probability distribution samples are drawn from and $Q(x_i, x_{i+1})$ is the proposal density. As mentioned, all the valid mass configurations have the same probability, thus P is a constant $\equiv 1$. Q has to be symmetric for

Markov chains. It is usually taken to be a multivariate Gaussian $\mathcal{N}(x, \hat{\boldsymbol{\Sigma}})$, where $\hat{\boldsymbol{\Sigma}}$ is an estimate of the true covariance matrix $\boldsymbol{\Sigma}$. In principle it could be estimated by an adaptive chain during the random walk, but then the chain is no longer Markovian as it loses the reversibility property. Therefore, first an initial adaptive burn-in phase is run to get an good estimate $\hat{\boldsymbol{\Sigma}}$, before the real MCMC random walk. In this way, a large ensemble of models can be generated. The estimation of the covariance matrix is refined in *GLASS* such that models are much less correlated. Further details and tests of the method can be found in Lubini & Coles (2012).

3.2 Priors and assumptions

Content:

• Describe what priors and assumptions we used

  To Do:

• Rephrase
• Maybe merge this subsection with previous subsection

We use different priors and assumptions to eliminate unphysical mass reconstructions of the lens. First of all, the densities κ_n need to be positive. As mass distributions with positive radial gradients are instable (CITATION NEEDED!), the density must always increase towards the center. Therefore, we require the local density gradient in every pixel except the central one to point towards the center within an angle of $50°$. The radial density profile decreases monotonically, as required.

To avoid large fluctuations in the density, we choose to add a smoothing prior. The density in any pixel except the central one is at most twice the average density of its neighboring pixels. If there is reason to expect an invariant distribution under a rotation by $180°$ (e.g. for doubles), we impose such a symmetry prior.

We also choose to include an additional external shear

$$\gamma_1 \left(\theta_x^2 - \theta_y^2\right) + 2\gamma_2 \theta_x \theta_y, \qquad (4)$$

which is added to (1) and the subsequent equations. We allow γ_1 and γ_2 to vary while fixing the maximum absolute value of the shear parameters. For doubles we fix the absolute value to be at most 10^{-2} (resp. 10^{-1} if no model could be generated for lower values —¿ find out which galaxy and write this in more detail).

We further assume that the lens and image positions are perfectly known. As the range of possible models is much larger than the errors on these quantities, this assumption is justified (Saha et al. 2006). We also fix a time order of the images. Furthermore, we choose a flat concordance cosmology with $\Omega_m = 0.28$, $\Omega_\Lambda = 0.72$, and $H_0^{-1} = 13.7$.

3.3 Shape measure

Content:

• Describe shape measure we use (same one as second GLASS paper)
• Say that it has been tested with mock lenses (second GLASS paper)

To Do:

- Rephrase
- Add formula how shape is defined
- Summarize results of test of second GLASS paper

To get a rough estimate of the shape of the surface mass distribution we use the inverse of the moment of inertia tensor of the mass map. Its eigenvectors and eigenvalues track the shape of the mass distribution. Thus, the shape is defined by two quantities; the ratio of the eigenvalues λ_1/λ_2, which describes the ellipticity, and the angle of the semi-major axis θ. This seemingly crude measure was tested on fake data and found to be working well. (INPUT HERE FAKE DATA TEST)

4 RESULTS

Content:

- Illustrate shape measure and reconstruction on PG1115 (with Tsevtkova time delays)
  - Describe different misalignment plots
  - Speculate what the plots could mean

To Do:

- Start from scratch for this section
- Use suggested structure (or think about better one)
- Selection of plots is probably fine, but both data points for the two different time delay estimates of PG1115

Structure of this section

- Reconstruction of PG1115
- Different ellipticities dark matter and stellar distribution
  - Misalignment stellar and dark matter distributions
- Alignment dark matter and group centroid (maybe merge with previous subsection)

For every lens 10000 models were generated. This number allows for reasonable statistics, while not being computationally too expensive. In general an external shear of $|\gamma_i|\,10^{-1}$ is required to model quads. *RXJ0911* and *MG2016* however, need a significantly larger external shear of $|\gamma_i| \sim 2 \cdot 10^{-1}$. This probably can be attributed to the cluster environments. As mentioned, the shear was limited to be $|\gamma_i| < 10^{-1}$ for doubles. The masses M_{dm} and $M_{tot} = M_{dm} + M_{stellar}$ are always the masses included up to the radius of the outermost image.

Surprisingly, the shape measure we define yields are well-constrained results, as can be seen in Figures 1 and 2. The errors, which are purely statistical, on the ellipticities and the angles of the semi-major axis do not dominate the result. Lenses with almost spherical halos, i.e. $\lambda_1/\lambda_2 \sim 1$, should however be treated with caution.

As mentioned in Section 2, there are different time delay estimates for *PG1115*. We find that the results do not change much when using different estimates. As can be seen in Figure 1 resp. Figure **??**, the dark matter distribution is a bit more spherical with the time delays from Tsvetkova et al. (2010) and the uncertainty on the angle of the semi-major axis grows. The significant misalignment we see is thus not affected by different time delays.
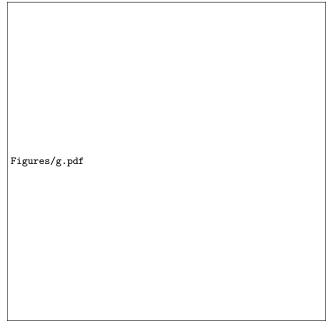

Figures/g.pdf

Figure 3. Misalignment of the dark matter halo and the direction of the centroid of the environment.

4.1 Misalignments between stellar and dark matter distributions

Figure 2 shows the differences between the angles of the stellar and the dark matter semi-major axes versus the ratio of the included dark matter and total mass. For lenses with a significant stellar component inside the outermost image radius, the distributions seem to be rather aligned. It seems that if the luminous mass is comparable to the dark matter mass, the distributions align. For a smaller stellar contribution this is not necessarily the case. The scatter increases and there can be significant misalignments, which can be seen especially clearly in the systems *PG1115* (also Figure 1) and *RXJ0911*. While alignments between the distributions are preferred, they do not seem to be the rule.

The environment might also play a role. Red are the systems, which are isolated and/or no group resp. cluster environment has been found yet, green the ones in such an environment. The misaligned systems are mainly the lenses with a known environment. Therefore, misalignments could be caused by the external effects.

4.2 Ellipticities of stellar and dark matter distributions

The ellipticities of the distributions versus the mass ratio are shown in Figure **??**. We see that every dark matter halo has a lower ellipticity λ_1/λ_2 and is thus closer to sphericity than the luminous part of the galaxy. The systems *B0712*, *B1152 HE1104*, and *MG2016* show especially large differences. It is not clear what could cause these discrepancies.

Figure **??** shows the misalignment versus the ellipticity of the dark matter halo. It is possible to roughly subdivide it into five different regions. Almost spherical halos with good alignment of the semi-major axes, almost spherical halos with good alignment of semi-major and semi-minor axes

Figure 1. Reconstruction of lens *PG1115*. The plots show the mean model of the generated ensemble of models. The coordinate system is centered on the lens galaxy. (a) shows the arrival time surface. The green dots are the images, the red curves are isochrones, and the black curve are the lemniscate resp. the limaçon. (b) shows the total matter distribution. The red circle marks the circle of the outermost image. The green resp. cyan ellipses mark the shape of the dark matter resp. stellar distribution. This shape is measured as described in Section 3.3. In this case, the shape of the total matter distribution (black) is indistinguishable from the dark matter distribution. (c) shows the dark matter distribution. The black lines show the median semi-major resp. semi-minor axis with 1σ- and 2σ- uncertainties. The solid pink line points to the group centroid with 1σ-uncertainties (dashed). (d) shows the luminous matter distribution.

(maximum misalignment between the semi-major axes), more elliptical, alligned halos, a seemingly 'forbidden' region for misalignments in between, and the upper right triangle, i.e. larger ellipticities and misalignments, which also seems forbidden. Understanding Figure **??** is certainly not trivial. Alignment with the semi-minor axis might be a stable configuration for almost spherical halos, while slightly smaller misalignments are unstable. The systems *Q0957*, *PG1115*, *B1422*, *MG2016*, and *HE2149* should be studied more closely as they could hold valuable information to decipher these relations.

4.3 Misalignments between the dark matter distributions and environment

Figure **??** we look at the alignment of the semi-major axes of the dark matter halos and vectors pointing to the centroid of the group or cluster or a companion galaxy. Although the error bars are huge, we see that five of these ten lenses, *Q0047*, *B0712*, *Q0957*, *PG1115*, and *B1422*, are probably aligned or at least consistent with the environment. The other half show slight misalignment.

Having a closer look at these lenses shows however that

at least two of them might in fact be aligned. For *RXJ0911* and *HE2149* there are no errors on the estimates of the centroid. Otherwise they would probably agree very well. *Q0047* does not seem to be aligned with the direction of the group centroid. The halo of *B1030* is almost spherical, so the apparent misalignment could maybe be explained. *MG2016* also has a known environment, is however not shown in this Figure as no estimate of the cluster centroid is given. There is however a high galaxy density towards the south-east, where also the cluster centroid probably lies. The halo seems to be roughly aligned with the cluster centroid.

We conclude that lenses in groups or cluster are probably aligned with the centroid, i.e. the center of mass, consistent with what one might expect naively. The light however needs not be as stated earlier.

5 CONCLUSION

Content:

- Quick overview of what was presented
- State again main results
- Say why this results are interesting

Figures/b.pdf

Figures/d.pdf

Figures/e.pdf

Figure 2. Plots of stellar and dark matter misalignments, ellipticities of the baryonic mass and dark matter distribution and a plot showing the ellipticity of the dark matter halo against the misalignment. Red symbols mark isolated objects or such without environment information, green symbols mark objects with at least one companion galaxy. In the second plot, stars denote the ellipticitie of the baryonic mass distribution, squares the ones of the dark matter halo.

• What is needed to understand such misalignments better (-¿ Surely need to understand environment effects better, ...)

To Do:

• Rephrase
• Maybe wait for final results

We used a nonparametric modelling method to reconstruct a total of 15 lenses. Using previously measured light maps, then converted to luminous mass maps Leier (2011),

we were able to isolate the dark matter distribution. We used the eigenvalues and eigenvectors of the inverse of the moment of inertia tensor to characterize the shape of the light and mass distributions. This allowed us to analyze the alignment between these distributions and the relation between the ellipticities. Furthermore, we included environment information, which we related the to the misalignment.

Our results can be summarized in the following way. If lenses lie in dense environments, mass and light need not be aligned. This might also be the case for lenses without

known environments. We found more scatter than previous analyses by Keeton et al. (1997), Koopmans et al. (2006), Treu et al. (2009), and Gavazzi et al. (2012) which all used SIEs mostly neglecting external shear to model the lenses. We also found that the semi-major and semi-minor axes of the distributions can be aligned, if the dark matter halos are close to sphericity. Up to our knowledge, this result was not obtained in other analyses.

We found that dark matter halos are rounder than the luminous galaxies, i.e. they have a lower eigenvalue ratio λ_1/λ_2. Previous analyses found a correlation between the ellipticities (Treu et al. 2009; Gavazzi et al. 2012), which we do not see. They also found a couple of cases, where the stellar distribution is more spherical than the dark matter halo. We claim that certain combinations of ellipticity of the dark matter halo and misalignment between light and mass seem to be forbidden. However, more lens systems are needed to support this claim.

We suspect that the dark matter halo might be aligned with the centroid of the group or cluster it lies in. Due to the large uncertainties in the centroid positions however, such alignments might as well be coincidences.

We want to stress again that the systems *SBS1520* and *PG1115*, which both show some misalignment and have time delay measurements, seem interesting enough to investigate further. In *SBS1520* we found that the outer parts of the dark matter distribution is rotated respective to the central, which displays an interesting feature possibly due a disc. It is on the other hand a very complicated system with a lot of structures along the line of sight. *PG1115* is easy to model, but still shows a clear misalignment. Thus, it could serve as a test for other methods that try to reproduce these misalignments.

6 ACKNOWLEDGEMENTS

REFERENCES

Angonin-Willaime M.-C., Soucail G., Vanderriest C., 1994, A&A, 291, 411

Auger M. W., Fassnacht C. D., Abrahamse A. L., Lubin L. M., Squires G. K., 2007, AJ, 134, 668

Auger M. W., Fassnacht C. D., Wong K. C., Thompson D., Matthews K., Soifer B. T., 2008, ApJ, 673, 778

Barkana R., 1997, ApJ, 489, 21

Burud I. et al., 2002, A&A, 383, 71

Burud I. et al., 2000, ApJ, 544, 117

Chartas G., Chuss D., Forman W., Jones C., Shapiro I., 1998, ApJ, 504, 661

Coe D., Fuselier E., Benítez N., Broadhurst T., Frye B., Ford H., 2008, ApJ, 681, 814

Coles J., 2008, ApJ, 679, 17

Courbin F., Lidman C., Meylan G., Kneib J.-P., Magain P., 2000, A&A, 360, 853

Eigenbrod A., Courbin F., Meylan G., 2007, A&A, 465, 51

Eulaers E., Magain P., 2011, A&A, 536, A44

Fassnacht C. D. et al., 1999, AJ, 117, 658

Fassnacht C. D., Cohen J. G., 1998, AJ, 115, 377

Fassnacht C. D., Lubin L. M., 2002, AJ, 123, 627

Fassnacht C. D., Xanthopoulos E., Koopmans L. V. E., Rusin D., 2002, ApJ, 581, 823

Faure C., Alloin D., Kneib J. P., Courbin F., 2004, A&A, 428, 741

Ferreras I., Saha P., Burles S., 2008, MNRAS, 383, 857

Ferreras I., Saha P., Williams L. L. R., 2005, ApJ, 623, L5

Garrett M. A., Walsh D., Carswell R. F., 1992, MNRAS, 254, 27P

Gavazzi R., Treu T., Marshall P. J., Brault F., Ruff A., 2012, ApJ, 761, 170

Grant C. E., Bautz M. W., Chartas G., Garmire G. P., 2004, ApJ, 610, 686

Hjorth J. et al., 2002, ApJ, 572, L11

Impey C. D., Foltz C. B., Petry C. E., Browne I. W. A., Patnaik A. R., 1996, ApJ, 462, L53

Keeton C. R. et al., 2000, ApJ, 542, 74

Keeton C. R., Kochanek C. S., Falco E. E., 1998, ApJ, 509, 561

Keeton C. R., Kochanek C. S., Seljak U., 1997, ApJ, 482, 604

Kneib J.-P., Cohen J. G., Hjorth J., 2000, ApJ, 544, L35

Kochanek C. S. et al., 2000, ApJ, 543, 131

Koopmans L. V. E., Treu T., Bolton A. S., Burles S., Moustakas L. A., 2006, ApJ, 649, 599

Kormann R., Schneider P., Bartelmann M., 1994, A&A, 284, 285

Lawrence C. R., Schneider D. P., Schmidt M., Bennett C. L., Hewitt J. N., Burke B. F., Turner E. L., Gunn J. E., 1984, Science, 223, 46

Lehár J. et al., 2000, ApJ, 536, 584

Leier D., 2011, PhD thesis, Astronomisches Rechen-Institut, Zentrum für Astronomie der Universität Heidelberg

Leier D., Ferreras I., Saha P., Falco E. E., 2011, ApJ, 740, 97

Lubini M., Coles J., 2012, MNRAS, 425, 3077

McKean J. P. et al., 2007, MNRAS, 378, 109

Momcheva I., Williams K., Keeton C., Zabludoff A., 2006, ApJ, 641, 169

Morgan C. W., Eyler M. E., Kochanek C. S., Morgan N. D., Falco E. E., Vuissoz C., Courbin F., Meylan G., 2008, ApJ, 676, 80

Morgan N. D., Chartas G., Malm M., Bautz M. W., Burud I., Hjorth J., Jones S. E., Schechter P. L., 2001, ApJ, 555, 1

Patnaik A. R., Narasimha D., 2001, MNRAS, 326, 1403

Raychaudhury S., Saha P., Williams L. L. R., 2003, AJ, 126, 29

Saha P., Coles J., Macciò A. V., Williams L. L. R., 2006, ApJ, 650, L17

Saha P., Williams L. L. R., 1997, MNRAS, 292, 148

Saha P., Williams L. L. R., 2004, AJ, 127, 2604

Schechter P. L., Moore C. B., 1993, AJ, 105, 1

Schneider D. P., Gunn J. E., Turner E. L., Lawrence C. R., Hewitt J. N., Schmidt M., Burke B. F., 1986, AJ, 91, 991

Shalyapin V. N., Goicoechea L. J., Gil-Merino R., 2012, A&A, 540, A132

Sluse D., Chantry V., Magain P., Courbin F., Meylan G., 2012, A&A, 538, A99

Toft S., Hjorth J., Burud I., 2000, A&A, 357, 115

Toft S., Soucail G., Hjorth J., 2003, MNRAS, 344, 337

Tonry J. L., Kochanek C. S., 1999, AJ, 117, 2034

Treu T., Gavazzi R., Gorecki A., Marshall P. J., Koopmans L. V. E., Bolton A. S., Moustakas L. A., Burles S., 2009, ApJ, 690, 670

Tsvetkova V. S. et al., 2010, MNRAS, 406, 2764

Warren S. J., Hewett P. C., Lewis G. F., Moller P., Iovino A., Shaver P. A., 1996, MNRAS, 278, 139

Williams K. A., Momcheva I., Keeton C. R., Zabludoff A. I., Lehár J., 2006, ApJ, 646, 85

Wisotzki L., Koehler T., Lopez S., Reimers D., 1996, A&A, 315, L405

Wong K. C., Keeton C. R., Williams K. A., Momcheva I. G., Zabludoff A. I., 2011, ApJ, 726, 84

Xanthopoulos E. et al., 1998, MNRAS, 300, 649

Yee H. K. C., 1988, AJ, 95, 1331

Yoo J., Kochanek C. S., Falco E. E., McLeod B. A., 2005, ApJ, 626, 51

APPENDIX A: RECONSTRUCTED LENSES

Lens	A	B	C	D	Symmetry	Point Masses
Q0047	1.083	1.083	1.083	1.083	Yes	$-\Delta\alpha = 2.301$, $-\Delta\delta = 2.301$, Mass range: $10^7 - 10^9 \mathrm{M_{Sun}}$
Q0142						
MG0414						
B0712						
RXJ0911						
BRI0952						
Q0957						
LBQS1009						
B1030						
HE1104						
PG1115						
B1152						
B1422						
B1608						
MG2016						
B2045						
HE2149						
Q2237						

Table A1. ...